Mathl. Comput. Modelling Vol. 17, No. 6, pp. 67–82, 1993
Printed in Great Britain.

0895-7177/93 $6.00 + 0.00

TEMPORAL MODEL OF AN OPTICALLY PUMPED CO-DOPED SOLID STATE LASER

T. G. WANGLER*
Department of Mathematics and Computer Science
Illinois Benedictine College, Lisle, IL 60532, U.S.A.
J. J. SWETITS
Department of Mathematics
Old Dominion University, Norfolk, VA 23508, U.S.A.
A. M. BUONCRISTIANI
National Aeronautics and Space Administration
Langley Research Center, Hampton, VA 23665, U.S.A.

(Received September 1991; revised and accepted September 1992)

Abstract—Currently, research is being conducted on the optical properties of materials associated with the development of solid-state lasers in the 2 micron region. In support of this effort, a mathematical model describing the energy transfer in a holmium laser sensitized with thulium is developed. In this paper, we establish some qualitative properties of the solution of the model, such as nonnegativity, boundedness, and integrability. A local stability analysis is then performed from which conditions for asymptotic stability are obtained. Finally, we report on our numerical analysis of the system and how it compares with experimental results.

INTRODUCTION

In the early 1980's, there was a renewal of interest in solid-state lasers, due in large part to the development and availability of new host materials. It was around this time that NASA began investigating tunable solid-state lasers as promising candidates for the Earth Observing System (Eos). During the past several years, research has been conducted on the sensitized holmium laser, which operates in the near infra-red region. It can be used as a source for both LIDAR (LIght Detection And Ranging) and DIAL (DIfferential Absorption and Lidar) as well as on aircraft to make Doppler lidar measurements of windshear since it operates in the eye-safe region.

In a solid-state laser, a dopant ion substitutes directly into the host lattice. When the lanthanide rare earth ion holmium (Ho) is used as a dopant in the host crystal yttrium aluminum garnet ($Y_3Al_5O_{12}$), the holmium ion substitutes into the yttrium sites. This induces a weak coupling to the host lattice that results in narrower absorption and emmision features than those commonly observed in transition metals. Although the holmium laser has high gain and good energy storage properties, ionic interactions among the holmium ions limit the concentration of holmium possible in any host; therefore, to increase the optical energy absorbed, a sensitizing ion is included. In the laser system under consideration, the lanthanide rare earth ion thulium (Tm) is used as a sensitizer for holmium. The interactions between thulium and holmium ions increase the efficiency of the Tm-Ho laser but at the cost of introducing more nonlinearities into the model. These nonlinearities make both the analysis and the laser dynamics significantly different than solid-state laser dynamics studied previously.

*Author to whom all correspondence should be addressed.

This work was supported by NASA/Langley Research Center. The project was overseen by Dr. Clay Bair, Dr. Phil Brockman, and Dr. Bob Hess in the Laser Technology and Applications Branch of FED. The financial support was provided by a fellowship (NGT-50346) under the NASA Graduate Researchers Program.

The model comprises thulium ions in energy levels $^3H_4$, $^3F_4$, and $^3H_6$; holmium ions in energy levels $^5I_5$, $^5I_7$, and $^5I_8$; and the photon density in the optical cavity. There are two main types of processes considered in the laser system; namely, those processes that are inter-ionic—involving the transfer of excitation from one ion to another—and those that are not. Inter-ionic processes include: cross relaxation, back transfer, and up-conversion. Processes that are not inter-ionic include: spontaneous emission, absorption, and stimulated emission. The model does not account for spatial dependence of excitation in the crystal rod, but rather utilizes a spacial average over the length of the rod.

In the next section, the system of equations for the electron populations and photon density is introduced and discussed. We then establish some qualitative properties of the solution to the system. After that, a local stability analysis is performed, and finally, the system is subjected to a numerical treatment and the numerical solution compared with experimental results obtained in the laboratory.

THE MODEL OF THE LASER DYNAMICS

The energy level diagram for the Tm^{3+} ion and the Ho^{3+} ion in YAG [1, Figure 2.1, p. 10] is the basis for the idealized model, Figure 1, of lasing action. For the remainder of the discussion, the following correspondence is made as a matter of notational convenience: thulium energy levels $^3H_6$, $^3F_4$, and $^3H_4$ correspond to energy levels 0, 1, and 2, respectively, and holmium energy levels $^5I_8$, $^5I_7$, and $^5I_5$ correspond to energy levels 0′, 1′, and 2′, respectively. The number of thulium ions, per cm^3, in energy level i and at time t will be denoted $N_i(t)$; $i = 0, 1, 2$. Similarly, the number of holmium ions, per cm^3, in energy level i' and at time t will be denoted $n_i(t)$; $i = 0, 1, 2$.

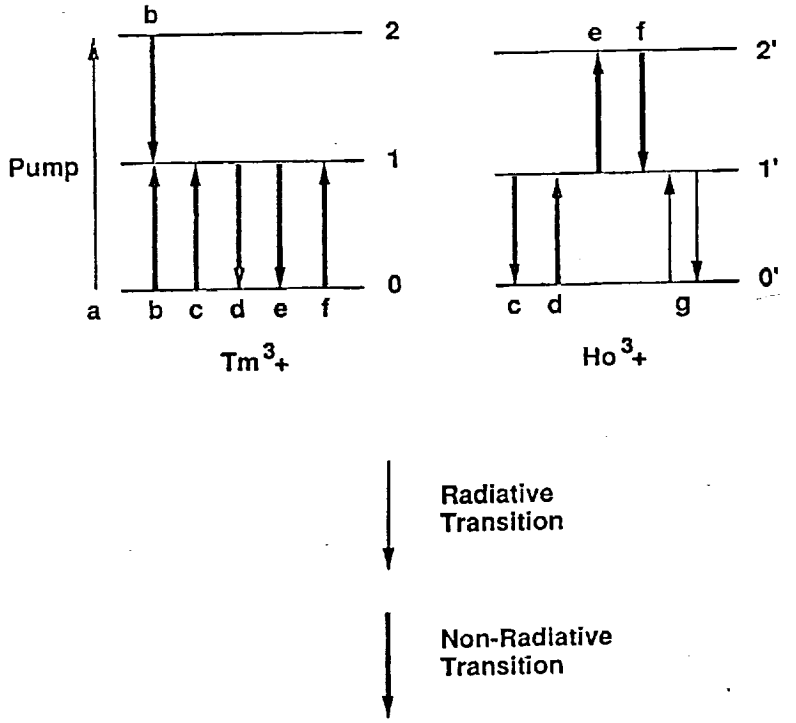

Figure 1. Idealized model of the Tm-Ho:YAG laser with the following processes represented: (a) stimulated absorption, (b) cross relaxation, (c) back transfer, (d) forward transfer, (e) up-conversion, (f) down-conversion, and (g) stimulated emission.

The temporal evolution of the dopant electron populations is described by the set of rate equations given by

$$\begin{aligned}
\frac{dN_2(t)}{dt} &= W_p(t)N_0(t) - \frac{N_2(t)}{\tau_2} - CN_0(t)N_2(t) \\
\frac{dN_1(t)}{dt} &= \frac{N_2(t)}{\tau_{21}} - \frac{N_1(t)}{\tau_1} + 2CN_0(t)N_2(t) + C_1^* N_0(t)n_1(t) \\
&\quad - C_1 N_1(t)n_0(t) + q_1' N_0(t)n_2(t) - q_1 N_1(t)n_1(t) \\
\frac{dN_0(t)}{dt} &= -W_p(t)N_0(t) + \frac{N_2(t)}{\tau_{20}} + \frac{N_1(t)}{\tau_1} - CN_0(t)N_2(t) \\
&\quad + C_1 N_1(t)n_0(t) - C_1^* N_0(t)n_1(t) + q_1 N_1(t)n_1(t) - q_1' N_0(t)n_2(t) \\
\frac{dn_2(t)}{dt} &= q_1 N_1(t)n_1(t) - \frac{n_2(t)}{\tau_2'} - q_1' N_0(t)n_2(t) \\
\frac{dn_1(t)}{dt} &= \frac{n_2(t)}{\tau_{21}'} - \frac{n_1(t)}{\tau_1'} + C_1 N_1(t)n_0(t) - C_1^* N_0(t)n_1(t) \\
&\quad + q_1' N_0(t)n_2(t) - q_1 N_1(t)n_1(t) - \sigma v\phi(t)\left(n_1(t) - \frac{g_1}{g_0}n_0(t)\right) \\
\frac{dn_0(t)}{dt} &= \frac{n_2(t)}{\tau_{20}'} + \frac{n_1(t)}{\tau_1'} + C_1^* N_0(t)n_1(t) - C_1 N_1(t)n_0(t) + \sigma v\phi(t)\left(n_1(t) - \frac{g_1}{g_0}n_0(t)\right).
\end{aligned} \tag{1}$$

In this system, C, C_1^*, C_1, q_1, and q_1' represent the probability of cross relaxation, back transfer, forward transfer, up-conversion, and down-conversion, respectively. All of these processes are depicted in Figure 1. The pumping rate is denoted by $W_p(t)$ and represents the number of photons, per microsecond, available to excite electrons in energy level 0 to energy level 2.

The quantities τ_i, τ_i' $i = 1, 2$ represent the spontaneous emission lifetime of energy level i, i', respectively. The quantity $1/\tau_{ij}$ represents the transition rate (due to spontaneous emission) from level i to level j. Similarly, $1/\tau_{ij}'$ represents the spontaneous emission transition rate from level i' to level j'. These two quantities satisfy the relations

$$\frac{1}{\tau_i} = \sum_{j=0}^{i-1} \frac{1}{\tau_{ij}} \quad \text{and} \quad \frac{1}{\tau_i'} = \sum_{j=0}^{i-1} \frac{1}{\tau_{ij}'} \qquad i = 1, 2.$$

The photon density is denoted by $\phi(t)$, and the rate equation describing the temporal evolution of the photon density in the optical cavity is given by

$$\frac{d\phi(t)}{dt} = v\sigma\phi(t)\left(n_1(t) - \frac{g_1}{g_0}n_0(t)\right) - \frac{\phi(t)}{\tau_c} + sp_o\frac{n_1(t)}{\tau_{fl}}. \tag{2}$$

Here, σ denotes the transition cross section, v is the velocity of light in the laser crystal, g_1 is the number of manifolds associated with energy level $1'$, and likewise for g_0. The contribution due to spontaneous emission of holmium ions in energy level $1'$ is denoted sp_o, and the fluorescent lifetime of the material is denoted τ_{fl}. The lifetime of a photon in the optical cavity is denoted by τ_c and can be expressed as [2]

$$\tau_c = \frac{2\ell_c/c}{-\ln R_1 R_2},$$

where ℓ_c is the length of the optical cavity, c is the velocity of light *in vacuo*, and R_1 and R_2 denote the reflectivity of the two mirrors. The electron populations of thulium and holmium are constrained by the relations

$$N_T = N_0(t) + N_1(t) + N_2(t) \quad \text{and} \quad n_T = n_0(t) + n_1(t) + n_2(t), \tag{3}$$

where N_T is the concentration of thulium ions, per cm^3, and n_T is the concentration of holmium ions, per cm^3.

These "population constraints" can be rewritten as

$$N_0(t) = N_T - N_1(t) - N_2(t) \quad \text{and} \quad n_0(t) = n_T - n_1(t) - n_2(t). \tag{4}$$

Substituting these expressions for $N_0(t)$ and $n_0(t)$ into system (1) reduces the system from six to four equations. Then, by including the rate equation for the photon density (2), we obtain

$$\begin{aligned}
\frac{dN_2(t)}{dt} &= W_p(t)(N_T - N_1(t) - N_2(t)) - \frac{N_2(t)}{\tau_2} - CN_2(t)(N_T - N_1(t) - N_2(t)) \\
\frac{dN_1(t)}{dt} &= \frac{N_2(t)}{\tau_{21}} - \frac{N_1(t)}{\tau_1} + 2CN_2(t)(N_T - N_1(t) - N_2(t)) \\
&\quad + C_1^* n_1(t)(N_T - N_1(t) - N_2(t)) - C_1 N_1(t)(n_T - n_1(t) - n_2(t)) \\
&\quad + q_1' n_2(t)(N_T - N_1(t) - N_2(t)) - q_1 N_1(t) n_1(t) \\
\frac{dn_2(t)}{dt} &= q_1 N_1(t) n_1(t) - \frac{n_2(t)}{\tau_2'} - q_1' n_2(t)(N_T - N_1(t) - N_2(t)) \\
\frac{dn_1(t)}{dt} &= \frac{n_2(t)}{\tau_{21}'} - \frac{n_1(t)}{\tau_1'} + C_1 N_1(t)(n_T - n_1(t) - n_2(t)) \\
&\quad - C_1^* n_1(t)(N_T - N_1(t) - N_2(t)) + q_1' n_2(t)(N_T - N_1(t) - N_2(t)) \\
&\quad - q_1 N_1(t) n_1(t) - \sigma v \phi(t) \left(n_1(t) - \frac{g_1}{g_0}(n_T - n_1(t) - n_2(t)) \right) \\
\frac{d\phi(t)}{dt} &= v\sigma\phi(t) \left(n_1(t) - \frac{g_1}{g_0} n_0(t) \right) - \frac{\phi(t)}{\tau_c} + sp_o \frac{n_1(t)}{\tau_{fl}}.
\end{aligned} \tag{5}$$

The coupled system (5) is the temporal model of the laser system expressed in terms of the physical variables. We now normalize system (5) to put it into the form used for the analysis and calculations in the subsequent sections. Hence, let

$$x(t) = \frac{N_2(t)}{N_T}, \quad y(t) = \frac{N_1(t)}{N_T}, \quad z(t) = \frac{n_1(t)}{n_T}, \quad w(t) = \frac{n_2(t)}{n_T}, \quad P(t) = \frac{\phi(t)}{\phi_{\text{norm}}} \tag{6}$$

be the normalized variables. Rewriting the rate equations (5) in terms of the normalized variables (6) yields

$$\begin{aligned}
\frac{dx}{dt} &= W_p(t)(1 - x - y) - \frac{x}{\tau_2} - D_1 x(1 - x - y) \\
\frac{dy}{dt} &= \frac{x}{\tau_{21}} - \frac{y}{\tau_1} + 2D_1 x(1 - x - y) + D_3 z(1 - x - y) \\
&\quad - D_2 y(1 - z - w) + D_6 w(1 - x - y) - D_7 yz \\
\frac{dw}{dt} &= D_8 yz - \frac{w}{\tau_2'} - D_9 w(1 - x - y) \\
\frac{dz}{dt} &= \frac{w}{\tau_{21}'} - \frac{z}{\tau_1'} + D_4 y(1 - z - w) - D_5 z(1 - x - y) \\
&\quad + D_9 w(1 - x - y) - D_8 yz - \beta_1[\gamma z + (1 - \gamma)(1 - w)]P \\
\frac{dP}{dt} &= \left\{ \beta_2[\gamma z + (1 - \gamma)(1 - w)] - \frac{1}{\tau_c} \right\} P + \beta_3 z
\end{aligned} \tag{7}$$

where

$$\begin{aligned}
D_1 &= CN_T & D_4 &= C_1 N_T & D_7 &= q_1 n_T & \beta_1 &= \sigma v \phi_{\text{norm}} \\
D_2 &= C_1 n_T & D_5 &= C_1^* N_T & D_8 &= q_1 N_T & \beta_2 &= \sigma v n_T \\
D_3 &= C_1^* n_T & D_6 &= q_1' n_T & D_9 &= q_1' N_T & \beta_3 &= \frac{sp_o n_T}{\tau_{fl} \phi_{\text{norm}}}
\end{aligned}$$

$$\gamma = 1 + \frac{g_1}{g_0}.$$

QUALITATIVE ANALYSIS

In this section, the full set of equations (7) is modified by excluding two physical processes—up-conversion and back transfer. This yields a simplified system for which certain qualitative properties of the solution are established. Throughout this discussion, the parameters are assumed to satisfy the following (physically realistic) relationships:

$$\begin{aligned} \tau_{21} > \tau_2 &> 0 \\ \tau_1 > \tau_{20} &> 0 \\ \tau_1' > \tau_c &> 0 \\ \beta_1, \beta_2, \beta_3 &> 0 \\ D_1, D_2, D_4 &> 0 \\ 1 &< \gamma \\ sp_o &<< 1. \end{aligned}$$

Excluding the above mentioned processes yields the following simplified system of rate equations

$$\begin{aligned} \frac{dx}{dt} &= W_p(t)(1-x-y)_+ - \frac{x}{\tau_2} - D_1 x(1-x-y)_+ \\ \frac{dy}{dt} &= \frac{x}{\tau_{21}} - \frac{y}{\tau_1} + 2D_1 x(1-x-y)_+ - D_2 y(1-z)_+ \\ \frac{dz}{dt} &= -\frac{z}{\tau_1'} + D_4 y(1-z)_+ + \beta_1(\gamma(1-z)_+ - 1)P \\ \frac{dP}{dt} &= \left\{\beta_2[1-\gamma(1-z)_+] - \frac{1}{\tau_c}\right\} P + \beta_3 z, \end{aligned} \tag{8}$$

where

$$\begin{aligned} (1-x-y)_+ &= \begin{cases} 1-x-y, & \text{if } 1-x-y \geq 0, \\ 0, & \text{otherwise,} \end{cases} \\ (1-z)_+ &= \begin{cases} 1-z, & \text{if } 1-z \geq 0, \\ 0, & \text{otherwise.} \end{cases} \end{aligned} \tag{9}$$

It follows directly from [3] that if (i) $W_p(t)$ is continuous, and (ii) the solution vector, $\mathbf{y} = [x, y, z, P]^T$, is bounded, then there exists a unique, continuous solution to the system (8). The following four theorems may be viewed as a validation of the model since they show that the solution to system (8) possesses the same kind of qualitative properties that one would expect the laser system to possess. Selected portions of the proofs are given below. The portions that are omitted can be found in [1, pp. 48–68]. The first theorem establishes the nonnegativity of the solution vector $\mathbf{y}$, as well as the ground states of thulium and holmium.

THEOREM 1. (NONNEGATIVITY). *If $W_p(t) > 0$ for $t > 0$ and $x(0) \geq 0$, $y(0) \geq 0$, $z(0) \geq 0$, and $P(0) \geq 0$, then*

(i) *If $1 - x(0) - y(0) > 0$, then $1 - x(t) - y(t) > 0$ for all $t > 0$;*
(ii) *If $1 - x(0) - y(0) < 0$, then there exists a T such that $1 - x(t) - y(t) > 0$ for all $t > T$;*
(iii) *(a) If $1 - x(0) - y(0) > 0$, then $x(t) > 0$ and $y(t) > 0$ for all $t > 0$*
(b) If $1 - x(0) - y(0) \leq 0$, then $x(t) \geq 0$ and $y(t) > 0$ for all $t > 0$;
(iv) *If $1 - z(0) > 0$, then $1 - z(t) > 0$ for all $t > 0$;*
(v) *If $1 - z(0) < 0$, then there exists a T^* such that $1 - z(t) > 0$ for all $t > T^*$;*
(vi) *$z(t) > 0$ and $P(t) > 0$ for all $t > 0$.*

Proof of Parts (i), (ii), and (iii) of Theorem 1

PROOF (i). Since $x(0) + y(0) < 1$, then by continuity of $x(t) + y(t)$, we know that $x(t) + y(t) < 1$ for t near zero. Suppose that at $t = T$, $x(T) + y(T) = 1$ and $x(t) + y(t) < 1$ for $0 \leq t < T$, then at $t = T$,

$$\frac{d}{dt}(x+y) = \left(-\frac{1}{\tau_2} + \frac{1}{\tau_{21}}\right) x + \left(-\frac{1}{\tau_1} - D_2(1-z)_+\right) y. \tag{10}$$

Now since $1/\tau_{21} - 1/\tau_2 < 0$ and $-1/\tau_1 - D_2(1-z)_+ < 0$, then if $x(T) \geq 0$ and $y(T) \geq 0$ and not both are zero, then from (10), $\frac{d}{dt}(x+y) < 0$ at $t = T$ which contradicts $x(t) + y(t) < 1$ for $t < T$ and therefore $x(t) + y(t) < 1$ for all t. Now since $x(T) + y(T) = 1$, not both x and y are zero at $t = T$; hence, it remains to be shown that $x(T) \geq 0$ and $y(T) \geq 0$.

Suppose $y(T) < 0$, then since $y(0) \geq 0$ and y is continuous, there exists a $T_y < T$ such that $y(T_y) = 0$ and $y(t) \geq 0$ for $0 \leq t \leq T_y$. Then at $t = T_y$

$$\frac{dy}{dt} = x\left[\frac{1}{\tau_{21}} + 2D_1(1-x-y)_+\right].$$

The quantity in brackets above is positive, so if $x(T_y) > 0$, then $\dot{y}(T_y) > 0$ which means y is increasing at $t = T_y$. But this contradicts $y(t) \geq 0$ for $0 \leq t \leq T_y$, and this contradiction implies $y(t) \geq 0$ for all t. Now suppose $x(T_y) < 0$, then since $x(0) \geq 0$ and x is continuous, there exists a $T_x < T_y$ such that $x(T_x) = 0$ and $x(t) \geq 0$ for $0 \leq t \leq T_x$. Then at $t = T_x$

$$\frac{dx}{dt} = W_p(T_x)(1-x-y)_+ > 0.$$

Hence, $\dot{x}(T_x) > 0$, which means x is increasing at $t = T_x$, which contradicts $x(t) \geq 0$ for $0 \leq t \leq T_x$. Therefore, $x(T_y) \geq 0$ and $x(t) \geq 0$ for $0 \leq t \leq T_y$. Now suppose $x(T_y) = 0$, then $\dot{y}(T_y) = 0$ and $\dot{x}(T_y) = W_p(T_y) > 0$. Additionally,

$$\begin{aligned}\frac{d^2y}{dt^2} = \frac{\dot{x}}{\tau_{21}} - \frac{\dot{y}}{\tau_1} + 2D_1 x\frac{d}{dt}(1-x-y)_+ + 2D_1\dot{x}(1-x-y)_+ \\ - D_2 y\frac{d}{dt}(1-z)_+ - D_2\dot{y}(1-z)_+,\end{aligned}$$

from which we obtain

$$\begin{aligned}\frac{d^2y}{dt^2}(T_y) &= \left(\frac{1}{\tau_{21}} + 2D_1\right)\dot{x}(T_y) \\ &> 0.\end{aligned}$$

So $y(T_y) = 0$, $\dot{y}(T_y) = 0$, and $\ddot{y}(T_y) > 0$. Hence, y is concave up at $t = T_y$, which implies that y is increasing to the right of $t = T_y$, and so

$$y(T) > 0. \tag{11}$$

Now suppose $x(T) < 0$, then since $x(0) \geq 0$ and x is continuous, we can choose $T_1 < T$ such that $x(T_1) = 0$ and $x(t) \geq 0$ for $0 \leq t \leq T_1$, then at $t = T_1$

$$\begin{aligned}\frac{dx}{dt} &= W_p(T_1)(1-x-y)_+ \\ &> 0,\end{aligned}$$

so x is increasing at $t = T_1$ which contradicts $x(t) \geq 0$ for $0 \leq t \leq T_1$; hence, the above supposition is false which implies $x(T) \geq 0$. This, together with (11), shows that at $t = T$

$$\frac{d}{dt}(x+y) < 0.$$

From prior comments, this implies that $x(t) + y(t) < 1$ for all t. ∎

PROOF (ii). The proof of (i) shows that if $x(0) + y(0) = 1$, then $x(t) + y(t) < 1$ for all $t > 0$. Suppose $x(0) + y(0) > 1$, then for t near zero

$$\begin{aligned}\frac{d}{dt}(x+y) &= \left(-\frac{1}{\tau_2} + \frac{1}{\tau_{21}}\right)x + \left(-\frac{1}{\tau_1} - D_2(1-z)_+\right)y \\ &< 0,\end{aligned}$$

since for t near zero $-1/\tau_2 + 1/\tau_{21} < 0$, $-1/\tau_1 - D_2(1-z)_+ < 0$, $x(t) \geq 0$, $y(t) \geq 0$, and not both are zero at $t = 0$. So $x(t) + y(t)$ is decreasing for t near zero. Now assume there exists a ξ such that $x(t) + y(t) \geq \xi > 1$ for all t, then

$$\begin{aligned}\frac{d}{dt}(x+y) &= \left(-\frac{1}{\tau_2} + \frac{1}{\tau_{21}}\right)x + \left(-\frac{1}{\tau_1} - D_2(1-z)_+\right)y \\ &= \left(-\frac{1}{\tau_2} + \frac{1}{\tau_{21}} + \frac{1}{\tau_1}\right)x - \frac{1}{\tau_1}(x+y) - D_2(1-z)_+ y \\ &\leq -\frac{1}{\tau_1}\xi,\end{aligned}$$

since $-1/\tau_2 + 1/\tau_{21} + 1/\tau_1 < 0$, $-D_2(1-z)_+ \leq 0$, and an argument similar to that given in (i) can be adduced to show that $x \geq 0$, $y \geq 0$. This inequality holds for all t, so upon integrating from 0 to t, we obtain

$$x(t) + y(t) - (x(0) + y(0)) \leq -\frac{1}{\tau_1}\xi t,$$

or equivalently,

$$x(t) + y(t) \leq -\frac{1}{\tau_1}\xi t + x(0) + y(0). \tag{12}$$

From inequality (12), and since $\tau_1 > 0$, it follows that

$$\lim_{t\to\infty}(x(t) + y(t)) = -\infty,$$

which contradicts $x(t) + y(t) \geq \xi > 1$ for all t. Hence, our assumption was false, which implies there exists a T such that $x(T) + y(T) = 1$ and $x(t) + y(t) < 1$ for t near T. The analysis from (i) now applies to show that $x(t) + y(t) < 1$ for all $t > T$ as required. ∎

PROOF (iii(a)). Let $x(0) + y(0) < 1$, then from (i), we know $x(t) + y(t) < 1$ for all t. Also, by hypothesis, $x(0) \geq 0$. Therefore, since x is continuous, $x(t) \geq 0$ for t near zero. Assume at some point, say $t = T_1$, that $x(T_1) = 0$ and $x(t) \geq 0$ for $0 \leq t \leq T_1$. Then at $t = T_1$,

$$\begin{aligned}\frac{dx}{dt} &= W_p(T_1)(1 - y(T_1))_+ \\ &> 0,\end{aligned}$$

which means x is increasing. This contradicts $x(t) \geq 0$ for $0 \leq t \leq T_1$. Hence, the above assumption is false, which implies $x(t) > 0$ for all $t > 0$.

Similarly, assume that at some point, say $t = T_2$, $y(T_2) = 0$ and $y(t) \geq 0$ for $0 \leq t \leq T_2$. Then at $t = T_2$, we have

$$\begin{aligned}\frac{dy}{dt} &= \overbrace{\left[\frac{1}{\tau_{21}} + 2D_1(1-x)_+\right]}^{\text{positive}} x \\ &> 0,\end{aligned}$$

since $x > 0$ and $1/(\tau_{21}) + 2D_1(1-x)_+ > 0$. This implies that y is increasing at $t = T_2$ which contradicts $y(t) > 0$ for $0 \leq t \leq T_2$. Hence, the assumption was fallacious which shows $y(t) > 0$ for all $t > 0$. ∎

PROOF (iii(b)). Let $x(0)+y(0) \geq 1$, then from (ii) we know there exists a T such that $x(t)+y(t) < 1$ for all $t > T$, and $x(T) + y(T) = 1$. Suppose that at $T_1 < T$, $x(T_1) = 0$ and $x(t) \geq 0$ for $0 \leq t \leq T_1$. Then at $t = T_1$

$$\frac{dx}{dt} = 0.$$

Also, at $t = T_1$ we have

$$\begin{aligned}\frac{d^2x}{dt^2}(T_1) &= -W_p(T_1)\dot{y}(T_1) \\ &= -W_p(T_1)\left[-\frac{1}{\tau_1}y(T_1) - D_2y(T_1)(1-z)_+\right] \\ &= W_p(T_1)y(T_1)\underbrace{\left[\frac{1}{\tau_1} + D_2(1-z)_+\right]}_{\text{positive}} \\ &> 0.\end{aligned}$$

Hence, x is concave up at $t = T_1$ and consequently increases to the right of it. From this, it follows that $x(t) \geq 0$ for $0 \leq t \leq T$; furthermore, for $t > T$ the analysis from (iii(a)) applies to show $x(t) > 0$ for all $t > T$.

Again, assume that at $T_2 < T$, $y(T_2) = 0$ and $y(t) \geq 0$ for $0 \leq t \leq T_2$, then at $t = T_2$

$$\begin{aligned}\frac{dy}{dt} &= \frac{1}{\tau_{21}}x(T_2) \\ &> 0.\end{aligned}$$

So y is increasing at $t = T_2$ which contradicts $y(t) \geq 0$ for $0 \leq t \leq T_2$; hence, the assumption was false which shows that $y(t) > 0$ for $0 < t \leq T$. Also, for $t > T$, the analysis from (iii(a)) pertains to show $y(t) > 0$ for $t > T$. Taken together, we have $y(t) > 0$ for all $t > 0$. ∎

The proofs for parts (iv), (v), and (vi) proceed along similar lines.

Theorem 1 states that the normalized ground levels of thulium and holmium remain nonnegative on $\mathcal{I} = [0, \infty)$, or, in other words, that the constraints (9) are self-enforcing. Consequently, we will drop the "+" subscripts in system (8) for the remainder of the discussion.

THEOREM 2. (INTEGRABILITY). *Let $W_p(t)$ be positive, continuous, and integrable on $\mathcal{I}$. Then if $x(0) \geq 0$, $y(0) \geq 0$, $z(0) \geq 0$, and $P(0) \geq 0$, then $x(t)$, $y(t)$, $z(t)$, and $P(t)$ are all integrable on $\mathcal{I}$.*

PROOF. Fix T such that $x(t) + y(t) < 1$ for all $t > T$, then for $t > T$ we have

$$\begin{aligned}\frac{dx}{dt} &= -\frac{x}{\tau_2} - D_1x(1-x-y) + W_p(t) - W_p(t)x - W_p(t)y \\ &= \left(-\frac{1}{\tau_2} - W_p(t)\right)x + W_p(t) - D_1x(1-x-y) - W_p(t)y \\ &\leq -\left(\frac{1}{\tau_2} + W_p(t)\right)x + W_p(t),\end{aligned}$$

since $W_p(t) > 0$, $y > 0$, $(1-x-y) > 0$, and $x \geq 0$. Rearranging, we get

$$\frac{dx}{dt} + \left(\frac{1}{\tau_2} + W_p(t)\right)x \leq W_p(t).$$

Now multiply both sides by $E(t) = e^{\int_T^t ((1/\tau_2) + W_p(\zeta))\,d\zeta}$ to obtain

$$E(t)\frac{dx}{dt} + \left(\frac{1}{\tau_2} + W_p(t)\right)E(t)x \leq E(t)W_p(t),$$

which implies

$$\frac{d}{dt}\{E(t)x(t)\} \leq E(t)W_p(t). \tag{13}$$

Upon integrating inequality (13) from $T \to t$ and noting that $E(T) = 1$, we obtain

$$E(t)x(t) - x(T) \leq \int_T^t W_p(u)E(u)\,du,$$

which holds for $t > T$. It now follows that

$$0 \leq x(t) \leq \int_T^t W_p(u)E(u)E^{-1}(t)\,du + x(T)E^{-1}(t). \tag{14}$$

Since

$$E(u)E^{-1}(t) = e^{-\int_u^t ((1/\tau_2)+W_p(\zeta))\,d\zeta},$$

we can express (14) as

$$0 \leq x(t) \leq \int_T^t W_p(u)e^{-\int_u^t ((1/\tau_2)+W_p(\zeta))\,d\zeta}\,du + x(T)e^{-\int_T^t ((1/\tau_2)+W_p(\zeta))\,d\zeta}.$$

Hence, integrating from $T \to s$ yields

$$0 \leq \int_T^s x(t)\,dt \leq \int_T^s \left\{ \int_T^t W_p(u)e^{-\int_u^t ((1/\tau_2)+W_p(\zeta))\,d\zeta}\,du \right\} dt + \int_T^s x(T)e^{-\int_u^t ((1/\tau_2)+W_p(\zeta))\,d\zeta}\,dt.$$

Now since W_p is continuous on $\mathcal{I}$, the order of integration may be interchanged to obtain the following equivalent expression

$$0 \leq \int_T^s x(t)\,dt \leq \int_T^s \left\{ \int_u^s W_p(u)e^{-\int_u^t ((1/\tau_2)+W_p(\zeta))\,d\zeta}\,dt \right\} du + x(T)\int_T^s e^{-\int_T^t ((1/\tau_2)+W_p(\zeta))\,d\zeta}\,dt. \tag{15}$$

Using the relation

$$\begin{aligned} e^{-\int_u^t ((1/\tau_2)+W_p(\zeta))\,d\zeta} &= e^{-\int_u^t W_p(\zeta)\,d\zeta} \cdot e^{-(t-u)/\tau_2} \\ &\leq e^{-(t-u)/\tau_2}, \end{aligned}$$

it follows from (15) that

$$\begin{aligned} \int_T^s x(t)\,dt &\leq \int_T^s W_p(u)\left\{ \int_u^s e^{-(t-u)/\tau_2}\,dt \right\} du + x(T)\left\{ \int_T^s e^{-(t-T)/\tau_2}\,dt \right\} \\ &= \int_T^s \tau_2 W_p(u)\left\{ 1 - e^{-(s-u)/\tau_2} \right\} du + x(T)\tau_2\left\{ 1 - e^{-(s-T)/\tau_2} \right\}. \end{aligned}$$

Since $\tau_2 > 0$ and $W_p(t)$ is integrable on $\mathcal{I}$, it now follows that $x(t)$ is integrable on $\mathcal{I}$.

To show that $y(t)$ is integrable on $\mathcal{I}$, start with

$$\frac{d}{dt}(x+y) = \left(-\frac{1}{\tau_2} + \frac{1}{\tau_{21}}\right)x - \frac{y}{\tau_1} - D_2 y(1-z) + D_1 x(1-x-y) + W_p - W_p x - W_p y$$

and proceed along the same general lines as above to establish that $(x + y)$ is integrable on $\mathcal{I}$. Then invoke the nonnegativity result for x and y to conclude that $y(t)$ is integrable on $\mathcal{I}$.

THEOREM 3. (BOUNDEDNESS). *If $W_p(t) > 0$ on $\mathcal{I}$, then $x(t)$, $y(t)$, $z(t)$, and $P(t)$ are all bounded on $\mathcal{I}$.*

THEOREM 4. *Let W_p, x, y, z, and P satisfy the hypotheses of Theorem 1. Furthermore, let $W_p(t) \to 0$ as $t \to \infty$. Then, the solution vector $\mathbf{y} \to 0$ as $t \to \infty$.*

STABILITY ANALYSIS

In this section, the equilibrium solutions are obtained, and a local stability analysis is performed. Before doing this, however, we make the simplifying assumption that the spontaneous emission term, sp_o, has a negligible affect on the asymptotic behaviour of the system and hence may be dropped. Furthermore, we will consider the case of continuous wave (CW) pumping. These two considerations are tantamount to taking $\beta_3 \equiv 0$ and $W_p(t) \equiv W_p$ in system (8), where W_p is a positive constant. Doing this yields the following system of rate equations:

$$\begin{aligned}
\frac{dx}{dt} &= W_p(1-x-y) - \frac{x}{\tau_2} - D_1 x(1-x-y) \\
\frac{dy}{dt} &= \frac{x}{\tau_{21}} - \frac{y}{\tau_1} + 2D_1 x(1-x-y) - D_2 y(1-z) \\
\frac{dz}{dt} &= -\frac{z}{\tau_1'} + D_4 y(1-z) + \beta_1[\gamma(1-z)-1]P \\
\frac{dP}{dt} &= \left\{\beta_2[1-\gamma(1-z)] - \frac{1}{\tau_c}\right\} P.
\end{aligned} \tag{16}$$

By setting the right hand side of equations (16) equal to zero, two equilibrium points are obtained. Equilibrium point 1 is denoted **I**, which has coordinates $(x^1, y^1, z^1, 0)$, and equilibrium point 2 is denoted **II**, which has coordinates (x^2, y^2, z^2, P^2), where the coordinates are given in terms of the physical parameters of the system.

Having located the equilibrium points, we now determine the stability properties of **I** and **II**. For the stability of **I**, introduce the new hat variables given by $\hat{x} = x - x^1$, $\hat{y} = y - y^1$, $\hat{z} = z - z^1$, and $\hat{P} = P - 0$. Linearizing system (16) about **I** yields

$$\dot{\hat{X}} = \hat{A}\hat{X} + \hat{g}, \tag{17}$$

where $\hat{A}$ represents the coefficient matrix of the linearized system, $\hat{X} = [\hat{x}, \hat{y}, \hat{z}, \hat{P}]^T$, and the $\hat{g}$ vector contains all the nonlinearities of the system.

Invoking the Routh-Hurwitz Theorem [1, pp. 71–73], the following necessary and sufficient condition for **I** to be asymptotically stable is obtained:

$$\beta_2[1-\gamma(1-z^1)] - \frac{1}{\tau_c} < 0.$$

The stability analysis for **II** parallels that of **I** and yields one condition for **II** to be asymptotically stable. The algebra associated with this condition, however, is tremendously complicated, and hence, we resort to a parametric investigation of the stability of the equilibrium points.

The numerics indicate there is an interplay of stability between **I** and **II**. To see this, we consider W_p as a parameter and choose it to be "small." Then using a computer program, we calculate the equilibrium values of **I** and **II** and use the Routh-Hurwitz criteria to determine the stability of each point. By gradually increasing W_p and repeating the process, we see there is an interchange of stability which goes like this: for W_p small, the P coordinate of **II** is negative, **II** is unstable, and **I** is asymptotically stable (i.e., no lasing). As W_p is increased, the P coordinate of **II** eventually reaches zero, and thus, the two equilibrium points coalesce (this is the threshold of lasing). Finally, as W_p is increased still further, the P coordinate of **II** becomes positive, **II** becomes asymptotically stable, and **I** becomes unstable (i.e., lasing occurs).

This is illustrated in Figure 2 where P^2 is graphed as a function of W_p, and the stability of **I** and **II** is noted. The value of W_p at which the interchange of stability occurs is a bifurcation point and is denoted W_p^*. From numerical calculations, we find $W_p^* \doteq 0.342 \times 10^{-5}$.

It is also of physical interest to see how the system responds as the cavity lifetime of a photon, τ_c, is varied. Choosing τ_c small and following the same procedure as above yields the same interplay of stability as before. Figure 3 gives P^2 as a function of τ_c, once again noting the stability of each point. From this, we see that τ_c has a bifurcation point which will be denoted τ_c^* and is approximated by $\tau_c^* \doteq 4.81 \times 10^{-5}$.

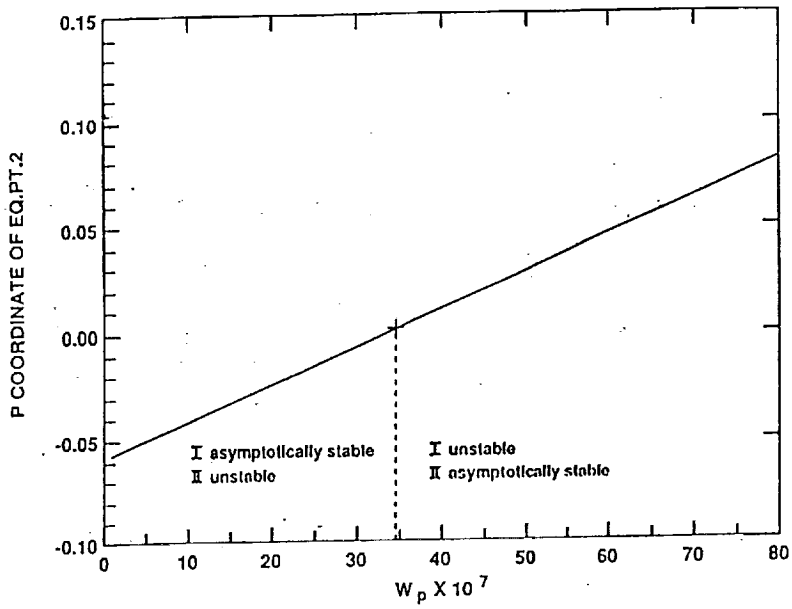

Figure 2. P coordinate of II as a function of the pumping term.

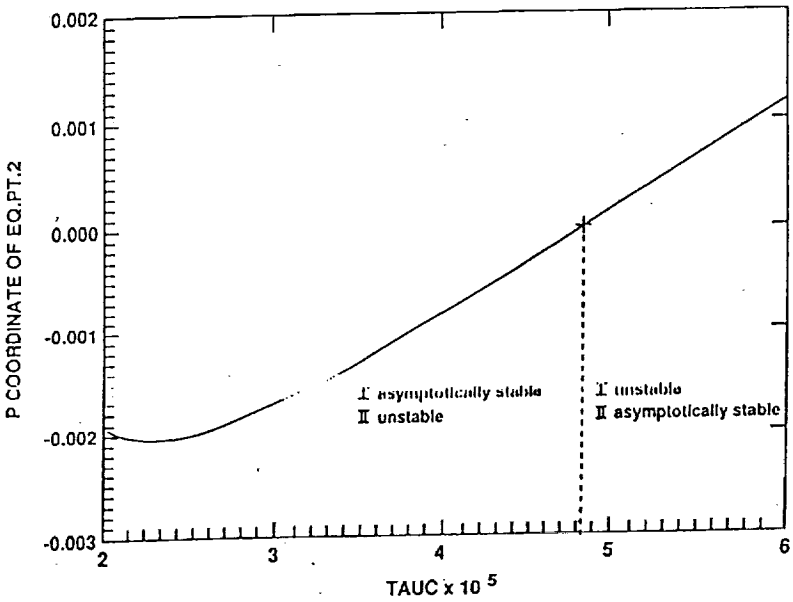

Figure 3. P coordinate of II as a function of the cavity lifetime τ_c.

NUMERICAL ANALYSIS

In this section, the numerical solution to system (8) is obtained. This is done by employing either the subroutine LSODA (when using a VAX 11/750) or the subroutine DDRIV2 (when using an IBM PC). In either case, all computations were performed in double precision arithmetic. LSODA was developed in 1987 at Lawrence Livermore National Laboratory in Livermore, California, by L. R. Petzold and A. C. Hindmarsh. DDRIV2 was developed in 1979 and revised in 1987 by D. K. Kahaner, National Bureau of Standards, and C. D. Sutherland of Los Alamos National Laboratory. Both subroutines were created for the numerical integration of stiff and nonstiff systems of first-order ordinary differential equations. When the system is stiff, the subroutines use a backward difference formula (BDF) to perform the numerical integration, and when the system is not stiff, they use a higher-order Adams method. Both LSODA and DDRIV2 have the capability of automatically switching from one method to the other as the system passes from stiff to nonstiff regions. The BDF method was chosen by both d.e. solvers throughout the interval of integration which indicates that system (8) is stiff. Roughly speaking, a system is

stiff when the characteristic equation of the associated linear system has a root with a "large" negative real part. A more detailed treatment of stiffness can be found in [4]. The numerical values of the system parameters are given in Table 1 and were used in the computation of the numerical solution. Employing the program in [1, Appendix B], the numerical solution of (8) was obtained. A typical example of the numerical solution is given in Figure 4 where the upper lasing level and the photon density are plotted. Since W_p is constant, a comparison of the "long time" behaviour of the numerical solutions with that of the equilibrium solutions can be performed. Using the parameter values in Table 1 and the Routh-Hurwitz criteria for asymptotic stability, it is found that **II** is asymptotically stable and **I** is unstable. The coordinates of **II**, as predicted by the stability analysis, are given in the left column below, and the numerical solutions at $t = 200\mu$s are given in the right column below.

$$\begin{aligned} x^2 &= 0.1304363 & x &= 0.1304372 \\ y^2 &= 0.7637408 & y &= 0.7637406 \\ z^2 &= 0.5238095 & z &= 0.5238095 \\ P^2 &= 0.0759492 & P &= 0.0759491 \end{aligned}$$

From this, it is evident that the d.e. solver captures the "long time" behaviour of the solutions extremely well.

Table 1. System parameters for Tm-Ho:YAG Laser.

$N_T = 1 \times 10^{21}/\text{cm}^3$	$\tau_{21} = 900\,\mu$s
$n_T = 1 \times 10^{20}/\text{cm}^3$	$\tau_1 = 11{,}000\,\mu$s
$\ell = 0.3\,\text{cm}$	$\tau_1' = 8{,}500\,\mu$s
$\phi_{\text{norm}} = 1 \times 10^{18}/\text{cm}^3$	$g_0 = 1$
$\ell_c = 17.5\,\text{cm}$	$g_1 = 1$
$R_1 = 1.0$	$\gamma = 2$
$R_2 = 0.95$	$\sigma = 7 \times 10^{-21}\text{cm}^2$
$C = \frac{1}{40 \times 10^{21}}\,\text{cm}^3/\mu$s	$q_1 = 0.0$
$C_1 = \frac{1}{475 \times 10^{20}}\,\text{cm}^3/\mu$s	$q_1' = 0.0$
$C_1^* = 0.0$	$v = 30{,}000\,\text{cm}/\mu$s
$\tau_2 = 450\,\mu$s	$\tau_c = 1 \times 10^{-3}\,\mu$s
$\tau_{20} = 900\,\mu$s	$W_p = 6 \times 10^{-3}/\text{cm}^3 \cdot \mu$s
	$sp_o = 1 \times 10^{-6}$

Various pumping schemes were considered in the model. Figure 5 gives the numerical solution for $P(t)$ when the pumping term is taken to be

$$W_p(t) = \alpha^2 t e^{-\alpha^2 t^2},$$

where $\alpha = .01133$. From this figure, we see that the photon density has irregular oscillations and decays rather rapidly, becoming negligible by about $t = 250\mu$s.

We now consider two modifications that are made to upgrade the model. The first is to include the terms that account for the back transfer of energy and that were excluded at the beginning of the section on qualitative analysis. The second is to replace β_2 and β_3 in the rate equation for the photon density with

$$\beta_2' = \left(\frac{\ell}{\ell_c}\right)\beta_2 \qquad \text{and} \qquad \beta_3' = \left(\frac{\ell}{\ell_c}\right)\beta_3.$$

The rationale for the second change is as follows. A mathematical model that accurately describes the dynamics of a laser system must account for both spatial and temporal variations in the dependent variables. Allowing for both types of variation yields a system of nonlinear partial

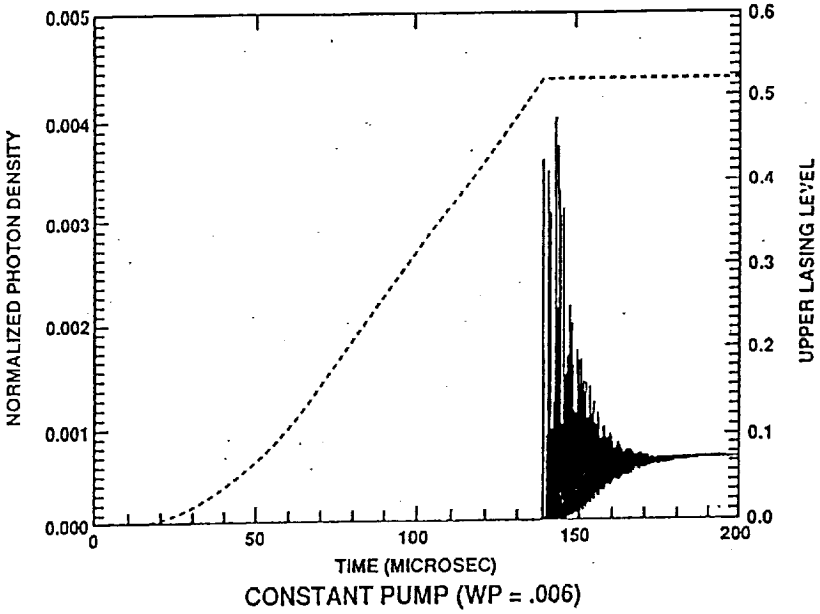

Figure 4. Normalized photon density and upper lasing level with a constant pump.

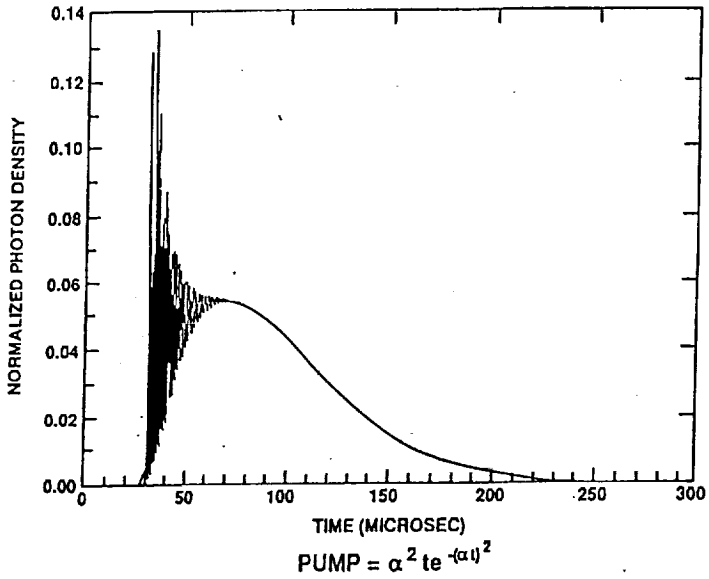

Figure 5. Normalized photon density with a decaying exponential pump.

differential equations (p.d.e.'). Due to the intractability of the equations and the amount of effort and computer time involved in solving the system numerically, various averaging techniques are used to eliminate the spatial dependence and thus make the system more tractable. L. F. Roberts *et al.* [5] gives three such averaging schemes along with their resultant o.d.e. models. The conclusion of this work is that only the temporal model obtained by taking a spatial average over the optical length of the cavity, ℓ_c, yields numerical results that agree qualitatively with those predicted by the spatial and temporal model. This averaging scheme can be incorporated into the model by replacing β_2 and β_3 by the quantities given above. Doing this and including the

back transfer terms yields the system

$$\begin{aligned}
\frac{dx}{dt} &= W_p(t)(1-x-y) - \frac{x}{\tau_2} - D_1 x(1-x-y) \\
\frac{dy}{dt} &= \frac{x}{\tau_{21}} - \frac{y}{\tau_1} + 2D_1 x(1-x-y) - D_2 y(1-z) + D_3 z(1-x-y) \\
\frac{dz}{dt} &= -\frac{z}{\tau_1'} + D_4 y(1-z) - D_5 z(1-x-y) + \beta_1[\gamma(1-z)-1]P \\
\frac{dP}{dt} &= \left\{\beta_2'[1-\gamma(1-z)] - \frac{1}{\tau_c}\right\} P + \beta_3' z.
\end{aligned} \tag{18}$$

The numerical solution to the system (18) was obtained giving special attention to the qualitative behaviour of the photon density for various values of C_1^* and ℓ/ℓ_c. Recall that C_1^* represents the probability of back transfer occurring. The pumping term was taken to be of the form

$$W_p(t) = \alpha^2 t e^{-\alpha^2 t^2}.$$

In Figure 6, the normalized photon density is graphed for a set of parameter values that are "close" to the values used in experimentation. Comparing Figure 6 with Figure 5, we see a salient disparity in the qualitative behaviour of the photon density. The previously observed erratic spiking has been replaced by regular and temperate oscillations. Figure 7 is a picture of the energy output of the laser system as displayed on the screen of an oscilloscope. By comparing Figure 6 with Figure 7, we see that the behaviour of the photon density, as predicted by the temporal model (18), is in remarkable agreement with the behaviour observed in the laboratory (both having about 7 oscillations in 25 μs).

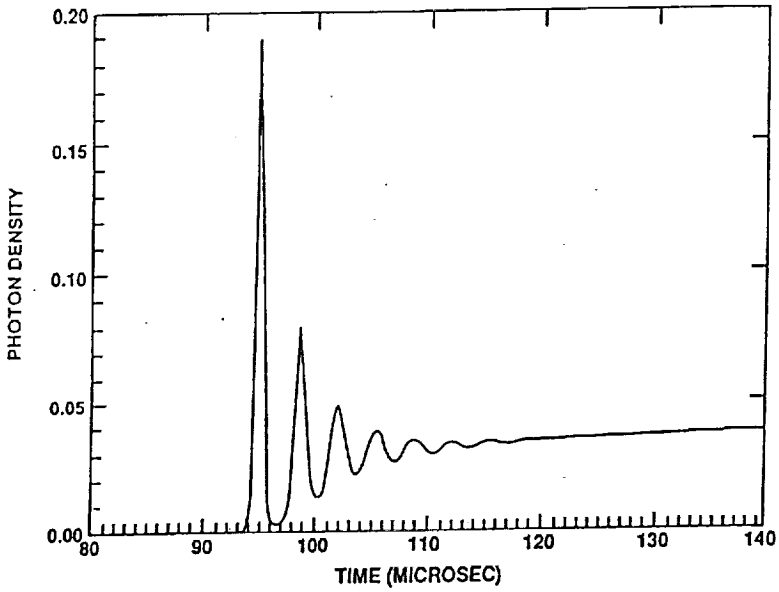

Figure 6. Photon density when using an alternate averaging technique.

Finally, we further upgrade the model by including the terms associated with the up-conversion of energy from the $^5I_7$ energy level to the $^5I_5$ energy level of holmium. This now brings us full-circle since we are back to the full set of equations (7) with the exception that β_2 and β_3 are replaced by β_2' and β_3', respectively, as defined above. The numerical solution to the system with up-conversion was computed taking the probability of up-conversion and down-conversion as

$$q_1 = 5.0 \times 10^{-22} \quad \text{and} \quad q_1' = 1.2 \times 10^{-23},$$

respectively. Figure 8 shows the interplay between the photon density and the upper lasing level of holmium, and Figure 9 gives a phase portrait of the same.

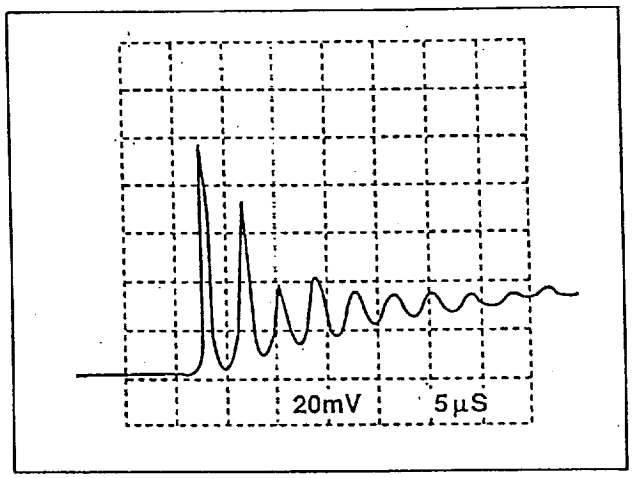

Figure 7. The energy output of the Tm-Ho:YAG laser as displayed on the screen of an oscilloscope.

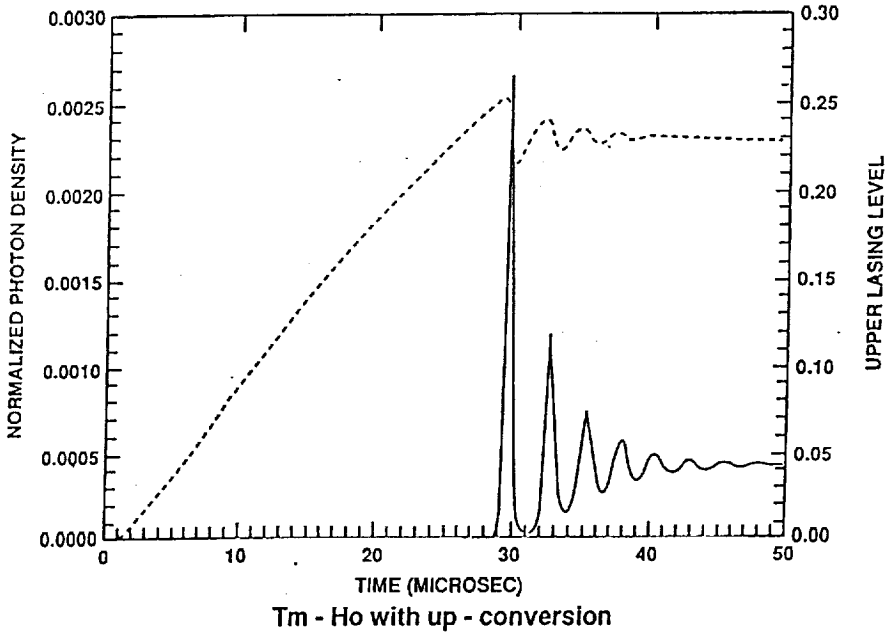

Figure 8. Upper lasing level and photon density with up-conversion included in the model.

SUMMARY AND CONCLUSIONS

We have developed a temporal model of the dynamics of an optically pumped co-doped six-level solid state laser. The model was developed to study the inter-ionic transfer of energy between thulium and holmium and how this affects the performance of the laser system. In this paper, we reported on the quantitative and qualitative behaviour of the solutions.

The validity of the simplified model was established by showing that—under appropriate conditions on the pumping term—solutions to the system exist and are bounded. Further, we showed that if the initial conditions are physically realistic and the pumping term is well-enough behaved, then the solutions are both nonnegative and integrable (integrability is desirable since calculating the efficiency of the laser system involves integrating over the photon density).

Two equilibrium solutions were obtained and a local stability analysis performed. The interplay of stability between the two equilibrium points was then demonstrated parametrically.

The system was solved numerically and found to be stiff. The d.e. solvers used performed exceptionally well and gave numerical solutions that agreed with the stability analysis and the experimental results. By gradually upgrading the simplified model, it was found that both back

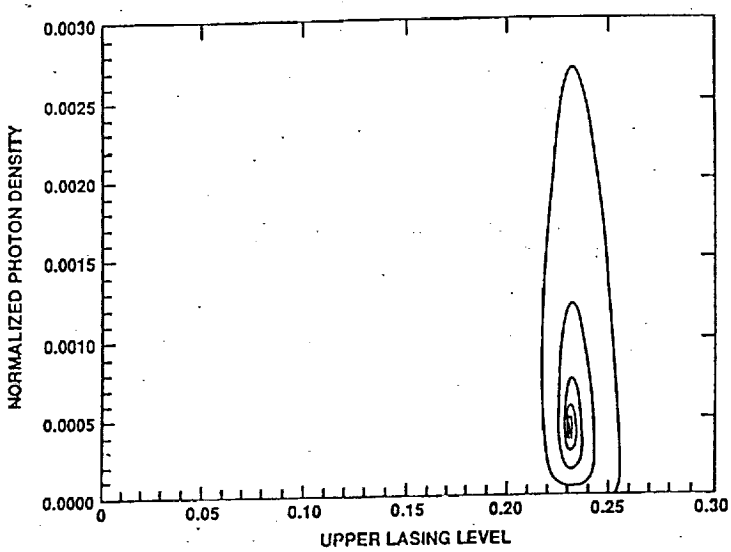

Figure 9. Phase portrait of the upper lasing level and the photon density.

transfer and up-conversion affect the time of lasing as well as the magnitude and frequency of the laser output, but it is an alternate averaging scheme that has the most dramatic affect on the qualitative behaviour of the output pulse.

REFERENCES

1. T.G. Wangler, Ph.D. Dissertation, Old Dominion University.
2. O. Svelto, *Principles of Lasers*, Plenum Press, (1989).
3. F. Brauer and J.A. Nohel, *Qualitative Theory of Ordinary Differential Equations*, p. 26, W.A. Benjamin Inc., (1969).
4. D. Kahaner, C. Moler and S. Nash, *Numerical Methods and Software*, pp. 284 ff, Prentice Hall, (1989).
5. L.F. Roberts, A.M. Buoncristiani and J.J. Swetits, An investigation of a mathematical model of the dynamics of an end-pumped Ti:Al_2O_3 Laser System (to appear).
6. D.A. Sanchez, *Ordinary Differential Equations and Stability Theory: An Introduction*, p. 57, Dover, (1979).